International Journal of Biological Macromolecules 219 (2022) 374–383

Contents lists available at ScienceDirect

International Journal of Biological Macromolecules

journal homepage: www.elsevier.com/locate/ijbiomac

# Electro and magnetoactive printed bi-functional actuators based on alginate hybrid hydrogels

Sheila Maiz-Fernández [a,b], Leyre Pérez-Álvarez [a,b,*], Iñaki Lopez de Munain-Arroniz [b], Aitana Zoco [b], Ana Catarina Lopes [b,c], Unai Silván [a,c], Daniel Salazar [a], José Luis Vilas-Vilela [a,b], Senentxu Lanceros-Mendez [a,c]

[a] BCMaterials, Basque Center for Materials, Applications and Nanostructures, UPV/EHU Science Park, 48940 Leioa, Spain
[b] Macromolecular Chemistry Group (LABQUIMAC), Department of Physical Chemistry, Faculty of Science and Technology, University of the Basque Country, UPV/EHU, Barrio Sarriena, s/n, 48940 Leioa, Spain
[c] Ikerbasque, Basque Foundation for Science, 48009 Bilbao, Spain

ARTICLE INFO

*Keywords:*
Alginate
Hydrogel
Soft actuator

ABSTRACT

Soft materials are attracting much attention for the development of biostructures able to mimic the movement of natural systems by remote actuation. Multi-sensitive hydrogels are among the best materials for obtaining dynamic and biocompatible soft structures for soft actuators and related biomedical devices. Nevertheless, bioinks based on naturally occurring and stimuli responsive hydrogels able to be 3D printed continues being a challenge for advanced applications. In this work 3D printable electrically and magnetically responsive, non-cytotoxic, hybrid hydrogels based on alginate and zero monovalent iron nanoparticles (NPs) are presented. The effect of NPs addition on the physico-chemical properties of the hydrogels is addressed, together with its effect on the functional electroactive and magnetoactive response. NPs concentration up to 10 % do not affect the mechanical stability of the gels, while promoting an increase actuation response.

## 1. Introduction

Soft robotics is an emerging field that has the potential to provide new solutions in the biomedical field, ranging from the development of minimally invasive surgical procedures to the delivery of drugs to otherwise inaccessible anatomical sites. The increasing applications of soft robots has promoted a great demand for bioinspired actuators in form of biocompatible and biodegradable polymers able to dynamically and reversibly change their shape [1]. In this regard, hydrogels capable of changing their form through the effect of a range of different external stimuli, including light [2], temperature [3], chemical environment [4] or by the application of magnetic [5] and electric fields [6] have been developed. The applicability and usability of soft actuators can be further enhanced by incorporating multifunctional shape-changing capabilities, that is, by integrating multiple actuation/sensing mechanisms within a unique soft hydrogel [7]. However, developing multifunctional materials that can be 3D printed is technically challenging, and generally 3D printable materials are largely monofunctional.

Hydrogels capable of reacting to magnetic fields have been introduced in biomedical applications in order to improve the biological activities of cells, tissues and organs, by the remotely regulation of the physical, chemical and mechanical properties of the biological microenvironment [8] or as biosensors [9]. Furthermore, recent studies have shown that magnetic hydrogels can serve as excellent drug targeting and controlled delivery systems, in particular in the area of magnetic hyperthermia treatment. Typically, magneto-sensitive materials are prepared by doping a material with magnetic nanoparticles (NPs) such as iron, cobalt or nickel [10]. Hydrogels disperse these particles and stabilize them inside their polymeric networks through physical interactions [5], making it possible to control the shape of the material and create remote motion by applying a magnetic field.

On the other hand, electroactive polymers change their size or shape when stimulated by an electric field, which, as it was the case of magnetic activation, can as well be applied remotely [11]. Among electroactive hydrogels, alginate has been widely used for biomedical applications due to its good biocompatibility, suitability to be injected,

* Corresponding author at: Macromolecular Chemistry Group (LABQUIMAC), Department of Physical Chemistry, Faculty of Science and Technology, University of the Basque Country, UPV/EHU, Barrio Sarriena, s/n, 48940 Leioa, Spain.
*E-mail address:* leyre.perez@ehu.eus (L. Pérez-Álvarez).

https://doi.org/10.1016/j.ijbiomac.2022.07.189
Received 3 June 2022; Received in revised form 19 July 2022; Accepted 23 July 2022
Available online 30 July 2022

and high versatility [12]. This hydrogel, which is composed of β-D-mannuronic (M) and α-L-guluronic (G) acids, is a linear anionic copolymer very abundant in nature, being found in the cell walls of brown marine algae and also being produced by some bacterial species [13]. Due to the presence of ionizable carboxylic acids in their structure, alginate hydrogels can change their shape reversibly through an external pH change or under the application of an electric field in the presence of electrolytes in the media. This response is based on the local swelling of a part of the hydrogel while the other contracts, causing the selective bending to one side. The most common way of obtaining alginate hydrogels is taking advantage of the specific and strong interactions between long stretches of G units and divalent or trivalent cations such as $Ca^{2+}$ or $Fe^{3+}$ [14]. This gelling mechanism takes place in very short times, and has been typically exploited to obtain 3D-printed structures [15,16]. Indeed, the increasing complexity of the geometrical properties required for the application of soft actuators in biomedicine greatly benefits from materials, which can be easily printed. This ability to obtain responsive materials with previously defined geometries and good spatial resolution enables the mimicking of the microenvironment of cells for biomedical applications, as well as the introduction of a new generation of functional materials [17].

Accordingly, in the present work, we present a new multifunctional 3D printable hybrid hydrogel based on alginate/$Ca^{2+}$ with magnetic iron zerovalent nanoparticles. Our results reveal that the developed material displays high biocompatibility, is suitable for injection and 3D printing, and exhibits high mechanical strength. Its time-dependent (4D) activation can be achieved by applying a magnetic or electric field, which gives the material great potential for the development of soft robotics and complex biomimetic applications.

## 2. Experimental methods

### 2.1. Materials

Sodium alginate was purchased from Sigma-Aldrich, iron zerovalent nanoparticles (Fe (0) NPs) coated by acrylic acid were obtained from NanoIron (NANOFER 25S) and calcium chloride ($CaCl_2$) was provided from Fisher Chemical. Sodium hydroxide (pure, pharma grade) and sodium phosphate monobasic (BioXtra, ≥99.0 %) were purchased from Sigma-Aldrich. All materials were used as received and solutions were prepared in deionized water.

### 2.2. 3D printing of hybrid hydrogels

Different amounts of iron zerovalent NPs (1, 2, 3, 5, 10 % *w*/w) were mechanically dispersed in 20 mL of deionized water. Then, sodium alginate was added to produce a 10 % w/w solution maintaining a moderate stirring without magnetization for 24 h. Once the solutions were prepared, they were loaded into the printer cartridges and different shapes were printed using an extrusion 3D printer (Cellink+, InkRedible+) onto a petri dish, which was previously covered by 1 M calcium chloride solution.

3D printing of the hybrid hydrogels strands was carried out in an extrusion 3D printer (Cellink+, InkRedible+). Strands of 10 % *w*/w alginate solution with a viscosity of 7048 cP were printed varying the diameter of the cartridge tip, the printing speed (300, 600 and 800 mm/min) and the injection pressure (25, 30, 35 and 40 kPa) in order to carry out the optimization of the printing parameters. Two different impression tips (Adhesive Dispensing Ltd) were used with an internal diameter of 0.41 and 0.254 mm. Finally, the diameters of the impressions were measured from a total of three strands at each condition using Fiji software. Printing was optimizing by analyzing by the uniformity factor (Eq. (1)) and the expansion ratio (Eq. (2)). The uniformity factor is defined as the difference between the lengths of the printed (l) and the designed structure (L):

$$Uniformity\ factor\ (U) = l/L \tag{1}$$

The expansion ratio (Eq. (2)) is defined as the relation between the diameter of the printed filament (d) and the theoretical diameter of the nozzle (D):

$$Expansion\ ratio\ (\alpha) = \frac{d}{D} \tag{2}$$

### 2.3. Physico-chemical characterization

Morphological and structural characterization. The microstructure of the printed structures was examined by scanning electron microscopy (SEM, Hitachi S-34000N). Printed alginate samples were lyophilized at −50 °C and −0.1 mbar, and then metallized with gold. Pore size analysis was performed with Fiji software by measuring ten pores from each section [18]. Hydrogel samples were also analyzed by transmission electron microscopy (TEM, Tecnai G2 20 Twin). On the other hand, Nicolet Nexus FTIR spectrometer (Thermo Scientific, Loughborough, UK) was used in order to study dried alginate hydrogels with and without Fe (0) NPs. All the experiments were carried out by ATR, at a resolution of 4 $cm^{-1}$ and 32 scans per spectrum. Finally, the crystallinity of the samples was studied by X-ray diffraction analysis (XRD, Bruker D8 Discover) with applying Cu-Kα radiation (1542 Å) at a 2**θ** range of 10–90° with voltage current settings of 40 kV and 40 mA, respectively.

Rheology: The dynamic rheological behaviour of alginate-Fe (0) based hydrogels was tested by oscillatory rheometry. The evolution of the storage (G′) and loss modulus (G″) was analyzed by frequency sweep measurements performed in a Rheometric Scientific Advanced Rheometric Expansion System (ARES), using parallel plate geometry (25 mm of diameter) with a gap distance of 1.5 mm at 25 °C. First, a shear strain sweep was recorded to determine the linear viscoelastic region. Then, frequency sweep measurements were carried out from 0.1 to 500 rad/s at a fixed strain of 1 %. Both strain and frequency sweeps were measured in triplicate.

Compressive stress/strain tests: Mechanical properties of the hybrid hydrogels were evaluated using and AEP Transducers, Metrotec. Hydrogel samples were printed with approximate dimensions of 20 × 3 mm and a thickness of 1 mm. The tensile test was performed using a 20 N load cell and a deformation speed of 10 mm/min. The elastic modulus of the samples was determined from the slope of the stress-strain curves in the range of 0–2 % strain. Mean values were calculated from results obtained for a minimum of 5 different samples. A one-way ANOVA test with Tukey's multiple comparison test was used for the statistical analysis. The statistical significant differences were considered at $p < 0.05$.

In vitro swelling: Synthesized hydrogels were lyophilized for one day at −50 °C and 0.1 mbar. Then, they were immersed at room temperature in phosphate buffer solution (PBS) (pH = 7.4) and the swelling ratio was calculated by weighing the hydrogels over time. The swelling factor of the hydrogels was calculated according to the Eq. (3).

$$Swelling\ factor = \frac{W_s - W_d}{W_d} \tag{3}$$

where, $W_s$ is the weight of the swollen hydrogels and $W_d$ is the weight of the dried hydrogels (each sample was analyzed in triplicate).

### 2.4. Bi-functional actuator response

Magnetic characterization and bending. The magnetization curves were carried out to determine the magnetic behaviour of the alginate hydrogels with different NPs contents by using a Vibrating Sample Magnetometer (Microsense EZ7-VSM). Hysteresis loops were obtained at room temperature under an applied magnetic field up to 1.8 T.

The response of the magnetic hydrogels to a constant magnetic field were carried out following the procedure described in [5]. Alginate strands were printed with different concentrations of NPs with a

cartridge tip diameter of 0.41 mm, a printing speed of 300 mm/min and a pressure of 25 kPa. Each strand was hung with the help of a clamp and activated using NdFeB alloy permanent magnet with a strength of 0.3 T. The magnet was placed at the end of the printed strand and the maximum displacement angle was determined. The force of the impact of the hydrogel on a flat surface as a consequence of the movement under the magnetic field was measured with a *Single Tact force* sensor, using an Arduino board to read the data.

A similar setup was implemented to evaluate the mechanical response of the hydrogels under different applied magnetic fields, in air or water media, and at room temperature. Well-localized constant fields were generated using VSM electromagnets as the magnetic field source and iron-based cores to intensify and homogenize the magnetic field in a gap of 3 cm. With the last configuration, it was ensured a spatial variation of the magnetic field of 1 T along the hydrogel strands with field steps of 0.2 T.

Electrical bending: The bending response of the hydrogels under electrical stimuli was also investigated. Printed hydrogel strands were placed in a 0.1 M NaCl solution between two platinum electrodes separated with a gap of 4 cm. A potential difference of 15 V was applied with a Hewlett Packard E3615A DC power supply (0–20 V) and images were acquired using a digital camera.

### 2.5. In vitro cytotoxicity assay

The biocompatibility of alginate-Fe (0) based hydrogels was evaluated by Live/dead assays. In brief, 24 h before the assay, $2.10^5$ cells/well mouse embryonic fibroblasts (MEFs) were plated in 24-well plates/well and cultured under normal conditions (37 °C and 5 % $CO_2$) in complete medium (DMEM containing 10 % fetal bovine serum and 1 % penicillin). Between 5 and 10 mg alginate hydrogels (with and without encapsulated NPs) were washed thoroughly with D-PBS, dried, and sterilized under UV light for 1 h before being added to the wells. After 24 h, hydrogels were discarded and cell cultures were washed with PBS and stained with Calcein-AM (2 μM), ethidium homodimer (EthD-1, 4 μM), and NucBlue (Thermo Fisher R37605, 2 drops/well). Fluorescence images of the blue (nuclei), green (cytoplasm of live cells), and red (nuclei of dead cells) channels were then acquired using a Leica DMi8 fluorescence microscope equipped with a 10× objective. Quantification of the collected data was performed using ImageJ software [18]. Cell viability was calculated as the ratio between red-stained nuclei and the total number of cells (blue-stained nuclei) in at least five images for three independent samples. Fluorescence in the green channel was used as a technical control.

## 3. Results & discussion

### 3.1. Hydrogel printability

The optimization of printing parameters was carried out by printing strands of alginate 10 % (*w*/w) in different printing conditions as can be seen in Fig. 1. The collected data reveal that both the expansion ratio and the uniformity factor of the printed strands are influenced by the extrusion pressure, the diameter of the nozzle tip and the printing speed. As expected, the injection tip with a 25 G nozzle (internal diameter of 0.254 mm) manages to print the lines with a smallest diameter which disfavor the expansion of the bioink through the surface (Fig. 1A). However, nozzle clogging derived from its small diameter causes the not reproducible printing of the strands, while using the 22 G nozzle (internal diameter of 0.41 mm) (Fig. 1B) reproducibility is achieved. It can be also observed that in all cases low printing speed and high pressure favor the bioink to spread, as the material has more time to spread, and more material is dispensed, respectively, leading to an increase in the expansion ratio. On the contrary, this conditions lead to the highest reproducibility, that is reflected in uniformity factor values closer to 1. These result are in good agreement with recently published studied related to these kind of materials [19]. Thus, to print with good fidelity and resolution, a 22 G nozzle, an intermediate pressure of about 25 kPa and a speed of 300 mm/min are required. These were the conditions used to print all alginate hydrogels in this work.

### 3.2. Morphological and physical characterization

Hydrogels are porous crosslinked structures, which can hold a large

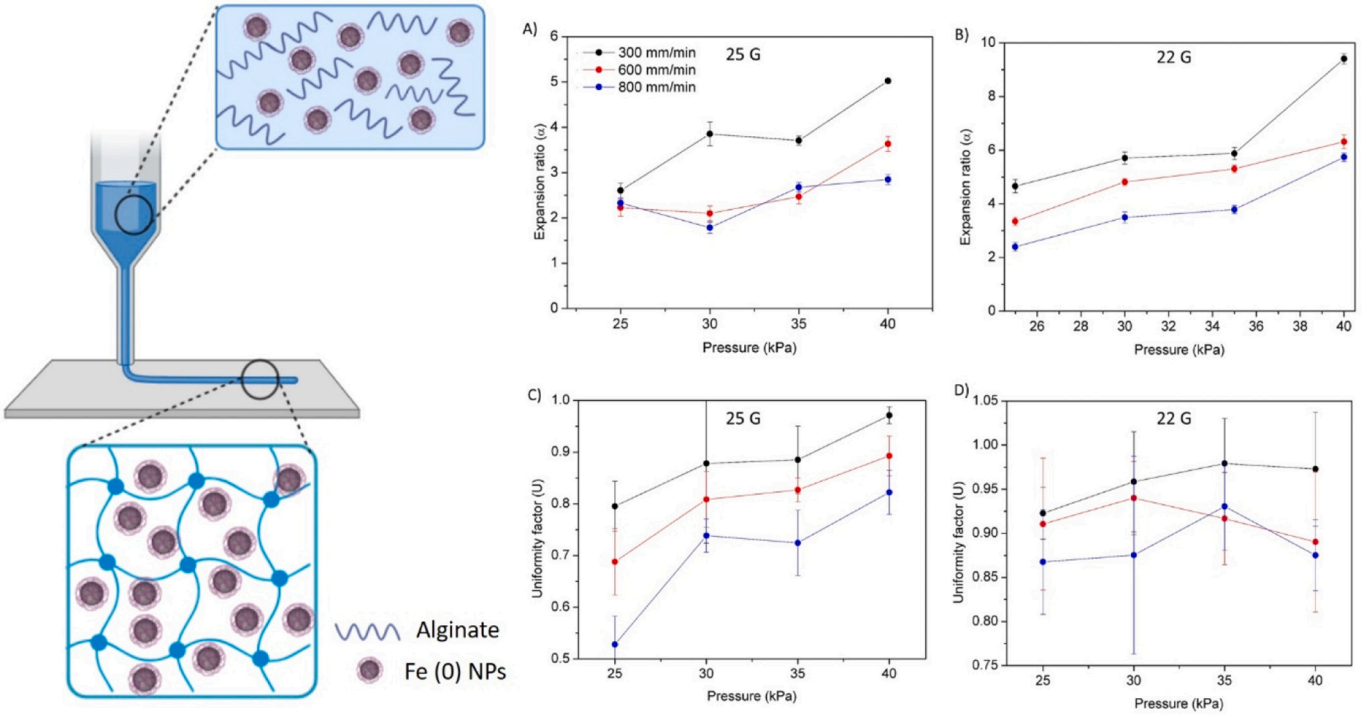


**Fig. 1.** Expansion factor of the printed structures with A) 25 G and B) 22 G noozle and uniformity factors of printed structure with a C) 25 G and D) 22 G noozles.

amount of water and other particles. Fig. 2A and B show representative SEM micrographs of a cross section of the printed alginate hybrid hydrogels. The gels reveal an interconnected porous microstructure with an average pore size of 56 ± 25 μm. Crystalline structures can be observed on the surface of the alginate printed strands (Fig. 2B) that correspond to salt ($CaCl_2$ and/or NaCl). TEM micrographs of pristine Fe (0) NPs dispersed in water (Fig. 2C) were compared to those within the prepared hybrid hydrogels. NPs do not maintain their spherical shapes and their initial size of 86 ± 30 nm is varied because of the formation of magnetic NP microclusters that are well dispersed within the hydrogel matrix (Fig. 2D). Despite the employed Fe (0) NPs being coated by an acrylic acid stabilizer layer to prevent oxidation, which facilitates their macroscopic dispersion in alginate solution, microscopic aggregates were observed that, however, do not compromise NPs macroscopic dispersibility.

Fig. 3A shows the XRD patterns of printed pristine and alginate/Fe hydrogels with different filler concentrations. Three characteristic peaks can be identified in all samples at 2θ of 31.975°, 44.855° and 45.654°. Peaks at 31.975° and 45.654° correspond to the presence of NaCl crystals [20], derived from the alginate matrix. The presence of this salt is a consequence of the use of $CaCl_2$ as gelling agent of sodium alginate solution. Chlorine crystallizes with sodium on the surface of the hydrogel matrix, as observed in the SEM micrograph (Fig. 2B), while calcium is coordinated by electrostatic interactions to the carboxylic groups of alginate. The peak shown at a 2θ diffraction angle of 44.855° is ascribed to the Fe (0) NPs and its intensity increases with increasing NP content in the hydrogels.

FTIR spectroscopy (Supplementary Fig. 1) allows to identify the characteristic absorption bands of alginate at 3700–3000 $cm^{-1}$ (O—H stretch), 1596 $cm^{-1}$ (antisymmetric C═O stretch), 1412 $cm^{-1}$ (symmetric C═O stretch), 1297 $cm^{-1}$ (skeletal vibration), 1010 $cm^{-1}$ (C—O—C antisymmetric stretch) as indicated in Lawrie et al. [21]. The addition of Fe (0) NPs within the hydrogels does not lead to any significant changes in the hydrogels spectra, independently of the filler content, indicating no chemical bonding between the polymer and the NPs.

The porous structure of alginate allows these composites to absorb and retain water. Fig. 3B indicates the swelling factor of the samples, showing that when low amounts of NPs (1–3 %) are added, the swelling factor of the hydrogels decreases, while higher percentages (5 and 10 %) lead to a swelling recovery. The swelling of a hydrogel is governed, together with the chemical composition, by the crosslinking density and the relaxation rate of the network. It has been reported that the addition of NPs on polymeric hydrogels can limit the relaxation rate and consequently acts as extra physical crosslinking [22]. On the other hand, it has been reported that increasing NPs addition restricts crosslinking density leading to the subsequent increase of swelling [23] (Fig. 3B). In this sense, low concentrations of NPs could hinders the absorption of liquid in the hydrogel supported by a limited relaxation of the network, while higher NPs amounts would lead to a reduced crosslinking density, promoting swelling [23].

### 3.3. Mechanical and rheological properties

The rheological characteristics of the prepared hydrogels was evaluated by frequency sweep tests at room temperature (Fig. 4A). All samples showed gel-like behaviour with a storage modulus (G′) higher than the loss modulus (G″) in all frequency range (Fig. 4), demonstrating that the binding between carboxylate groups in the G-blocks of the polysaccharide and $Ca^{2+}$ divalent cations has been successfully established, leading to form strong hydrogels [24].

Further, a considerable increase of G′ and G″ is observed for the hybrid hydrogels, when compared with pristine alginate hydrogels. Comparatively, the introduction of zero-valent iron nanoparticles to the "egg-box" structure, typically created between alginate and calcium, results in materials with an improvement of their mechanical properties. Quantitatively, these properties are 10 times higher than hydrogel based solely on alginate/$Ca^{2+}$. These results are in agreement with those

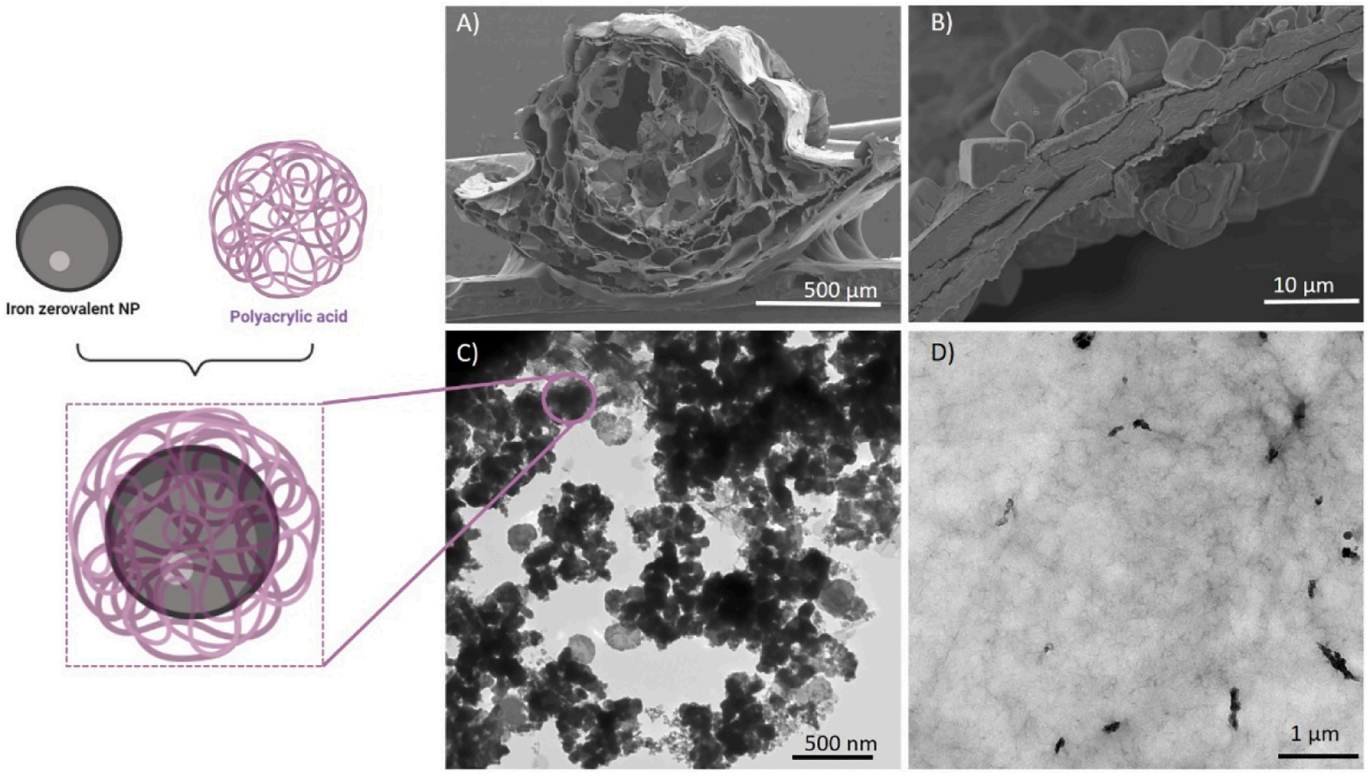


**Fig. 2.** A) Representative SEM micrograph of alginate hydrogels without NPs, B) SEM image of salt crystals on the surface of alginate hydrogels, C) TEM image of Fe (0) NPs in aqueous dispersion and D) TEM image of Fe (0) NPs within the alginate matrix.

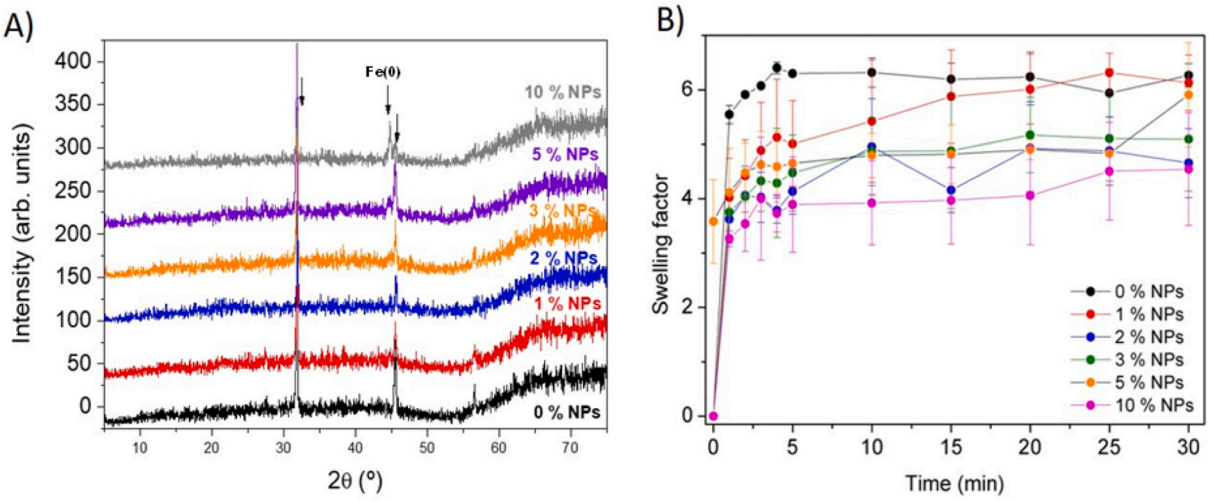


**Fig. 3.** A) X-Ray diffraction spectra of alginate samples with different concentrations of Fe (0) NPs and B) Swelling of alginate samples with different NPs concentrations.

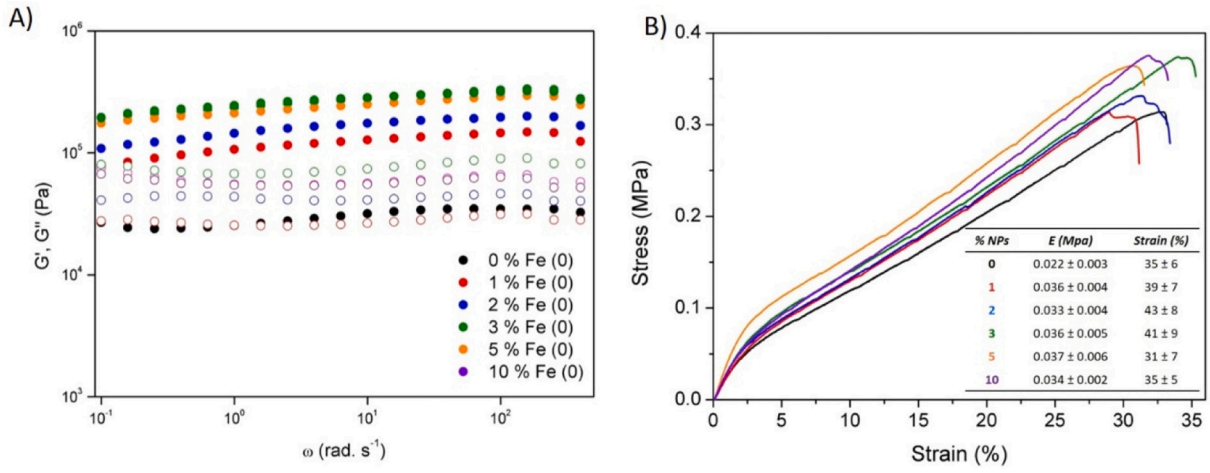


**Fig. 4.** A) Rheological response: Storage modulus (G′, filled circles) and loss modulus (G″, open circles) of the samples with different filler content and B) Effect of Fe (0) NPs on the stress-strain tensile mechanical properties of alginate.

reported in the literature for similar hybrid hydrogels [22].

As the introduction of inorganic fillers in polymeric systems allows to tune the mechanical properties of hydrogels to specific applications [25], the influence of Fe (0) NPs on the Young's modulus and on the maximum deformation of the gels was evaluated in tensile tests. Fig. 4B shows typical tensile stress-strain curves for alginate hydrogels with different filler contents. The collected data reveal that the Young moduli increase with the addition of the filler, from 0.022 MPa for pristine alginate to 0.034 MPa for the composite sample with 10 % filler content. However, the variation of the filler content does not play a relevant role on determining the mechanical properties in the concentrations under evaluation. That is, the addition of Fe (0) NPs leads to stiffer and less elastic hydrogels in all the cases. In addition, it is observed that regardless of the filler content, hybrid hydrogels present similar profiles and Young moduli, corroborating rheological results. Consequently, it can be concluded that the introduction of NPs, which confer the magnetic response to the material, does not imply a great alteration of the mechanical properties of the hydrogels.

### 3.4. Bi-functional actuator response

#### 3.4.1. Magnetic properties and actuation

Magnetic properties of the hydrogel samples were characterized by the measurement of the hysteresis loops (Fig. 5A). A comparative analysis of the curves show an increase of the saturation magnetization values from 0 to 3.9 $A{\cdot}m^2{\cdot}kg^{-1}$ when the NPs content increases from 0 % to 10 % *w*/w. The absence of hysteresis observed for all hydrogels demonstrate that they still are in a superparamagnetic regime for the 86 nm size NPs, without remanent magnetization upon removal of the magnetic field. No change in the shape of the loops indicates that the NPs did not degrade or decompose during processing.

The magnetic hysteresis loops (Fig. 5A) show that the maximum saturation magnetization of the magnetic hydrogels embedded with Fe (0) NPs exhibits a noticeable decline compared to that of the pure Fe (0) NPs (saturation magnetization of pure iron: 217 $A{\cdot}m^2{\cdot}kg^{-1}$ [26]) which is associated to the magnetic dilution of NPs in the hydrogel matrix. Also, the magnetic response is enhanced by increasing the concentration of Fe (0) NPs in the alginate matrix, the saturation magnetization of the magnetic hydrogel with 10 % of NPs reaching 3.9 $A{\cdot}m^2{\cdot}kg^{-1}$, which is about 5-fold higher than the value obtained with 1 % of NPs, which is 0.8 $A{\cdot}m^2{\cdot}kg^{-1}$ (Fig. 5B). The non-linear behaviour of the saturation

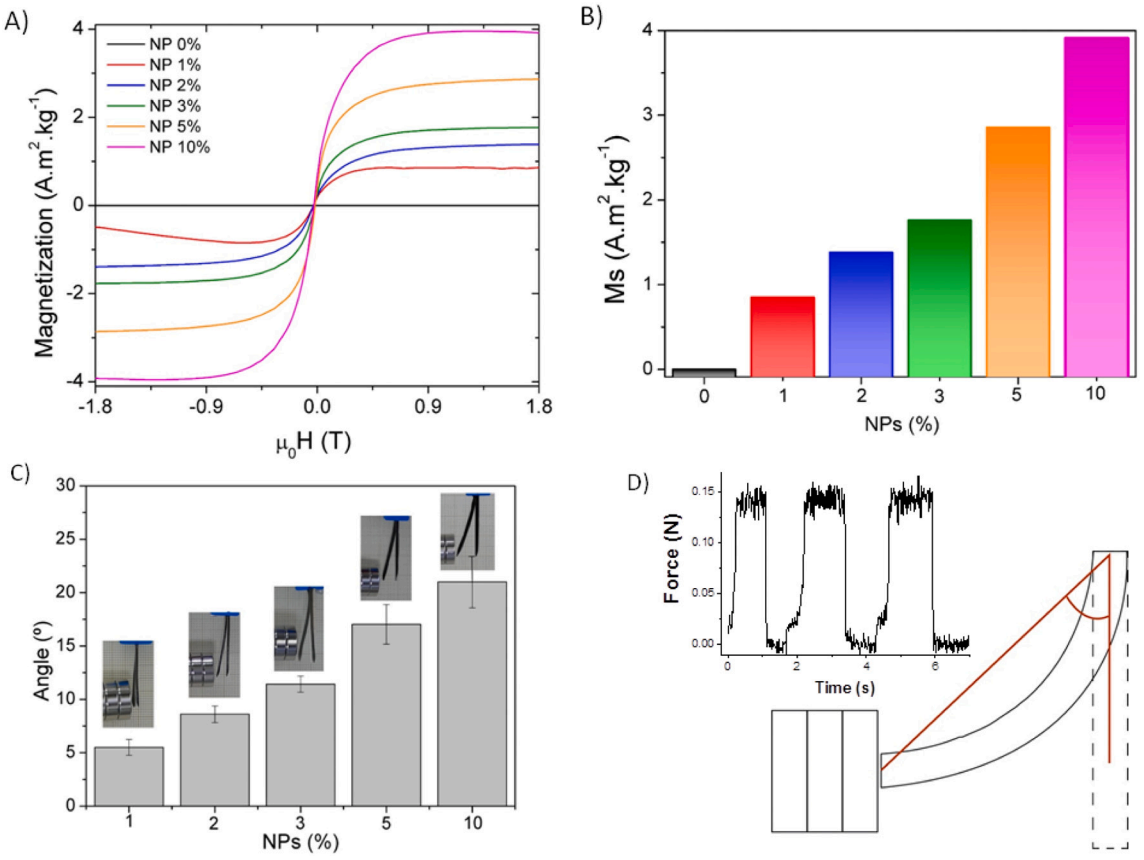


**Fig. 5.** A) Magnetic hysteresis loops of alginate hydrogels with Fe (0) NPs and B) Saturation magnetization values as a function of filler concentration, C) Displacement angle under applied magnetic field using a neodymium permanent magnet (0.3 T) and D) Impact force measured as function of time with the approximation of the magnet to hydrogels with 10 % of NPs and illustration for its determination, as well as for that of the displacement angle.

magnetization can be related to an inhomogeneous distribution of NPs in the hydrogels. In fact, values of saturation magnetization can be used to determine a more realistic concentration of NPs content. Considering the value of saturation magnetization of the pure iron zerovalent nanoparticles covered by PAA as 128 A·m$^2$·kg$^{-1}$ [27] an estimation of the experimental concentration of the filler within the hydrogels is presented in Table 1. The results show that the processing of the hydrogel results in a NPs loss possibly due to segregations during mixing (Table 1).

Typically, the enhanced magnetic properties of hybrid hydrogels compromise their stretchability and toughness [28], and the balance of the mechanical characteristics and magnetic properties of magnetic hydrogels is still considered a challenging issue [28]. However, here presented hydrogels display a significant increase in their magnetic properties while their mechanical properties remain almost invariable.

Hydrogels' magnetic response was employed to promote their bending actuation. To measure the bending response, printed alginate strands were exposed to a neodymium alloy permanent magnet (0.3 T) positioned 10 mm from one end of the printed samples. The other end was held without an external field (Video 1; Supplementary material).

**Table 1**
Estimation of the experimental concentration of Fe (0) nanoparticles in the prepared different hydrogels.

| Nominal concentration of NPs (%) | 1 | 2 | 3 | 5 | 10 |
|---|---|---|---|---|---|
| Ms (A·m$^2$ kg$^{-1}$) | 0.85 ± 0.18 | 1.38 ± 0.22 | 1.76 ± 0.25 | 2.86 ± 0.33 | 3.91 ± 0.40 |
| Real concentration (%) | 0.66 ± 0.18 | 1.07 ± 0.22 | 1.37 ± 0.25 | 2.23 ± 0.33 | 3.05 ± 0.40 |

With this configuration, the maximum displacement and curvature angles were measured for the hydrogels with different NPs concentration (Fig. 5D). Fig. 5C shows how the bending angle increases with increasing concentration of NPs in the hydrogel. That value increases from 5 to 20°, for the samples with 1 % and 10 % of NPs, respectively. Furthermore, the force of the impact of hybrid hydrogel on a flat surface was determined using a *Single Tact* force sensor. It was stick on a glass surface, which in turn was placed between the samples and the magnetic field. The results (inset Fig. 5D) show that the impact of the force of samples with the highest NPs content reaches a value of 0.15 N.

The potential of prepared hydrogels as soft printed actuators was further proven by analyzing the motion generated in the presence of a varying magnetic field (0–1 T) in air and water (Video 2, Supplementary material) with 1 and 10 % of Fe (0) NPs content (Fig. 6).

As shown in Fig. 6 and Supplementary Fig. 2 the movement of the soft printed actuators increases with the addition of iron zerovalent content as well as with the applied magnetic field, reaching maximum displacement angles above 20° both in air and water.

### 3.4.2. *Electrical actuation*

Due to their polyelectrolyte nature, the developed hydrogels can also act as electrical actuators and deform in the presence of an external electric field. The bending behaviour of printed alginate strands towards the cathode was studied by applying a potential difference of 15 V through platinum electrodes. It should be noticed that this bending movement is reversible when the direction of the electric field is changed, as shown in Fig. 7 and Video 3, Supplementary material.

When a potential difference is applied, electrolysis of the NaCl solution takes place. At the cathode (negative pole), $OH^-$ groups are generated and $H_2$ gas is released, while at the anode (positive pole) $Cl^-$

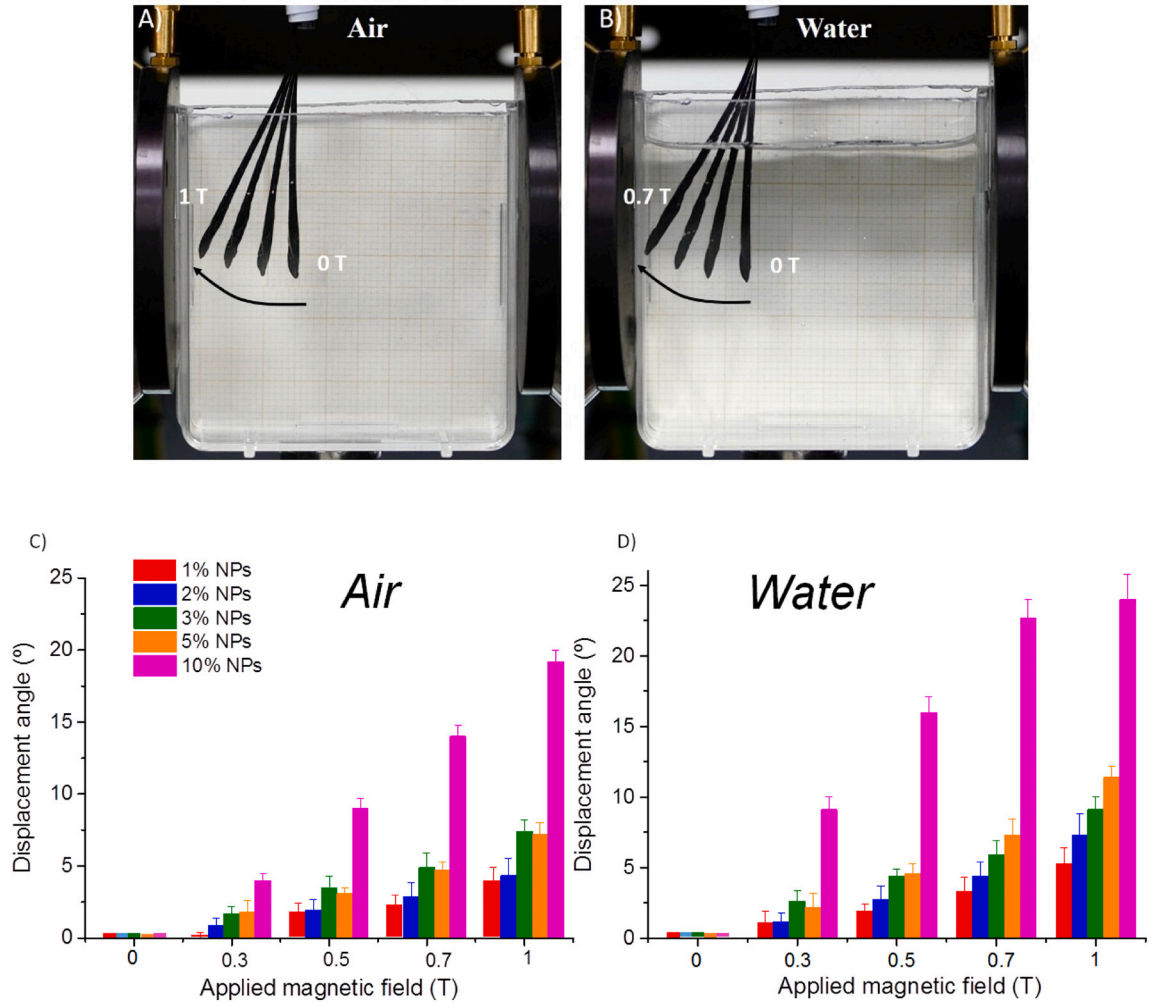


**Fig. 6.** Motion generated in the printed actuators with 10 % of Fe (0) NPs in air A), and in aqueous medium B), in the presence of a varying magnetic field (0–1 T). Histogram of displacement angles vs magnetic field both air and water.

anions are consumed and $Cl_2$ gas is released.

$$\text{Anode}: 2Cl^- \rightarrow Cl_{2\,(g)} + 2e^-$$

$$\text{Cathode}: 2H_2O + 2e^- \rightarrow H_{2\,(g)} + 2OH^-$$

The hydroxyl groups generated move from the cathode to the anode, while the sodium ions in the solution are moved to the cathode. The carboxylic groups of the printed alginate actuator that is placed between both electrodes, at pH ~ 6.5 are present in their ionic form (—$COO^-$). Thus, the electrostatic repulsion between carboxylate groups of the polymeric network is responsible for the swelling of the alginate hydrogel. The concentration of $OH^-$ groups increases on one side of the alginate strand that faces the negative electrode, and the hydrogel acts as a semipermeable membrane where the difference in the concentration of hydroxyl ions on different sides of the membrane generates the osmotic pressure to increase across it. Due to this increase in osmotic pressure, the hydroxyl ions generated begin to cross the membrane and accumulate on the positive electrode, causing the hydrogel to swell on the side that is closest to the anode. Therefore, the alginate hydrogel bends towards the cathode (negative electrode). Different mechanisms have been proposed to explain this behaviour of polyelectrolyte networks [29]. For instance, the bending in the Coulomb mechanism is attributed to the movement of the ions inside the gel, being the most common mechanism for hydrogels that are in a non-electrolytic environment [11]. However, in alginate samples when the potential difference is applied in deionized water, without NaCl electrolyte, the bending is not appreciated, that discloses the importance of this type of mechanism. On the other hand, the electrochemical mechanism can also explain the bending of the alginate actuators as is shown in Fig. 7. This mechanism takes into account the changes in pH that occur in the medium due to the electrolysis of NaCl solution [29]. With the application of the external electric field between the two electrodes, the amount of hydroxyl ions in the cathode begins to increase, increasing the pH in this area (blue colored pH paper in Fig. 7D). Then, as the $OH^-$ ions move towards the anode, the pH increases in the positive electrode (Fig. 7E). According to this mechanism, the basic pH finally accumulated at the anode causes the swelling of the area closest to it, leading to the bending towards the cathode side (Fig. 7A).

Finally, the dynamic enrichment/depletion mechanism considers the interaction of mobile counter ions ($Na^+$) with ionized carboxylic groups. Once the voltage is applied, the electrolyte counter ions ($OH^-$ and $Na^+$) migrate towards electrodes of opposite charges. Nevertheless, in the middle of the way the negatively charged alginate actuator side is placed. $Na^+$ ions pass through the hydrogel to the negative electrode, interacting with the carboxylic groups closest to that area. This reduces the repulsive forces between —$COO^-$ groups and thus, the local deswelling on the hydrogel part facing the negative electrode takes place and the gel bends towards the cathode [11].

In other words, in this anionic system, the $OH^-$ ions cause a swelling in the hydrogel and the $Na^+$ counterions generate a deflation in the

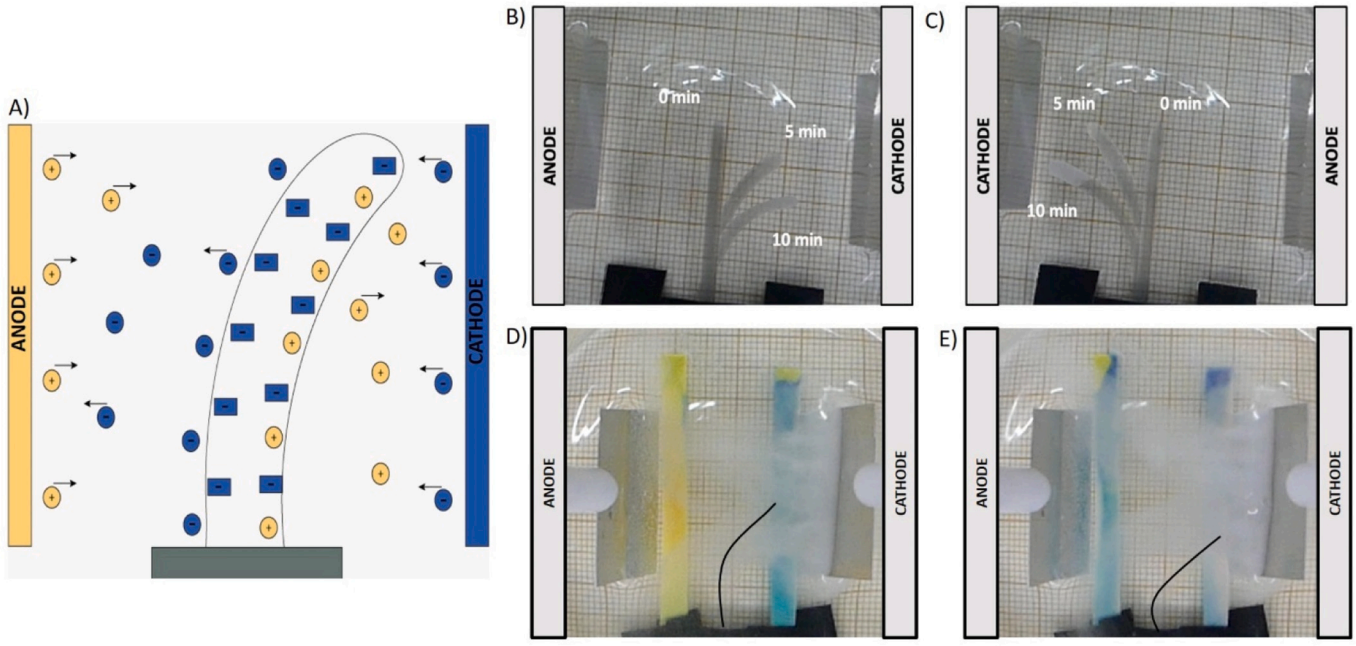


**Fig. 7.** A) Scheme of the charges present in the bending of the alginate strands. B) Displacement of the alginate printed actuator in 10 min under an applied potential of 15 V. C) Displacement of the alginate printed actuator by reversing the electric field. D) pH in the environment of the alginate actuator after 50 s of starting the electrolysis with a potential of 15 V. E) Variation of the pH after 3 min of starting electrolysis.

hydrogel. These two effects cause the alginate to bend towards the cathode. However, sometimes in the beginning of the electrolysis it can be observed how the gel bends towards the anode. This takes place because the $OH^-$ ions have not yet passed through the gel, so swelling is generated in the cathode area causing a bending towards the anode. However, after a few seconds, the $OH^-$ ions begin to accumulate in the anode and the movement of the hydrogel shifts towards the cathode (Fig. 8A).

On the other hand, Fig. 8B shows the displacement achieved by the alginate magnetic composite actuators during 10 min applying a potential difference of 15 V. It is observed that the increase in the concentration of NPs positively influences the electromechanical response of the material. This is attributed to the fact that the NPs are coated by acrylic acid (—$COO^-$ moieties) that prevent them from oxidizing and help in their dispersion in the alginate matrix. Increasing the amount of NPs also increases the amount of charges (—$COO^-$) within the hydrogel, which enhances the effect of the mechanism corresponding to the dynamic enrichment/depletion by improving the bending of the hydrogel. In hydrogels with low NPs content (1, 2, 3 and 5 %) no significant difference ($p < 0.05$) is observed in the angle of displacement, however, an

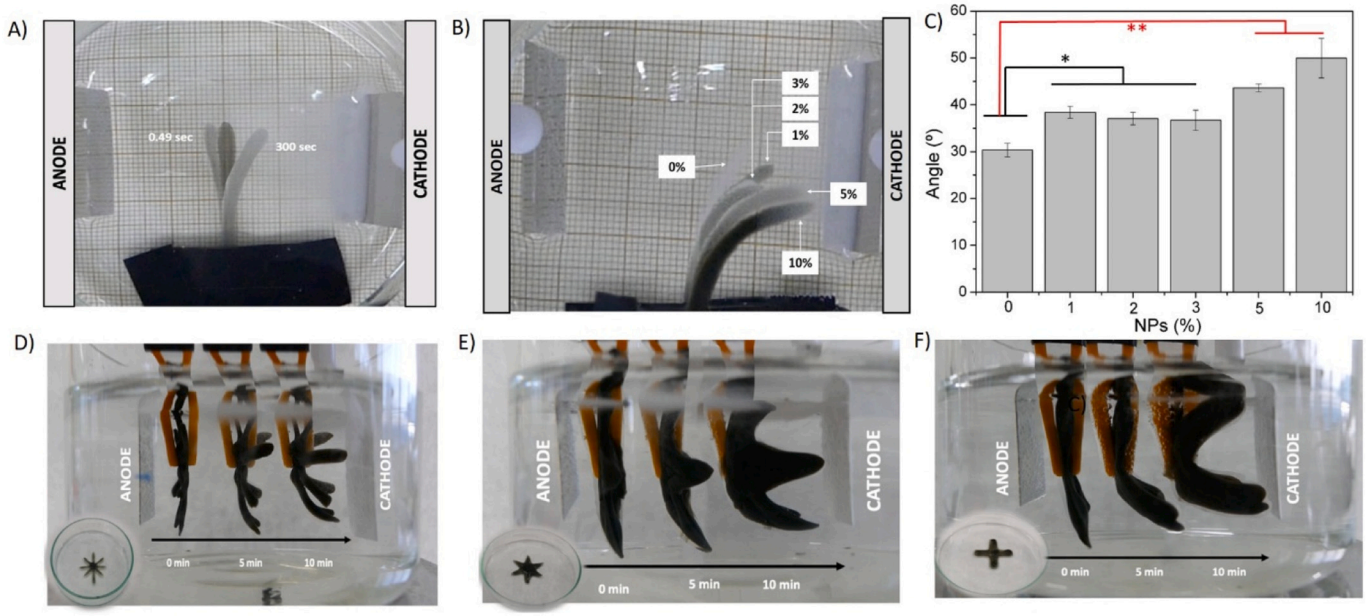


**Fig. 8.** A) Hydrogel bending over time, B) Maximum bending of the prepared hybrid alginate hydrogels with different nanoparticles content and C) Histogram of the obtained displacement angles. One-way ANOVA test with Tukey's multiple comparison test was used for the statistical analysis ($p < 0.05$). (*) No significant differences and (**) Significant differences. D–F) Bending response of alginate hydrogels with different geometries D) Asterisk E) Five-pointed star and F) Cross.

increase to 10 % of Fe (0) NPs leads to a significantly higher bending angle (Fig. 8C).

The difference in the mechanism of action of both stimuli was proven by the sequential performance of a dual stimulation (Supplementary Fig. 3). In the presence of the magnet and without electric field, the bending promoted by the magnetic effect is cancelled along the time by an electric effect carried out in the opposite bending direction (Supplementary Fig. 1 A–C and E–G), leading to the same bending angle expected in the absence of the magnetic field regardless the NPs content in the hydrogels. However, when the sequence starts by the electric effect (Supplementary Fig. 1 D and H), this is, when the local swelling/deswelling of the hydrogels has already taken place, the magnetic action of the NPs in the opposite direction does not significantly vary the bending of the strand but slows down the motion. This dual actuation (magnetic and electric) can be used to finely tune the deformation of the hydrogels.

The applicability of printable hybrid hydrogels as electromechanical soft actuators was further explored with more complex structures, including cross, asterisk and five-pointed stars, where printability and electric actuation for pristine alginate and hybrid hydrogels was corroborated under an applied voltage of 15 V (Fig. 8C–D and Video 4, Supplementary material).

### 3.4.3. *In vitro cytotoxicity assay*

To estimate possible cytotoxic effects of the hydrogels, the survival rates of murine embryonic fibroblasts (MEFs) after 24 h contact with alginate gels with and without nanoparticles was evaluated. Staining of cell nuclei with EthD-1, only possible in case of disrupted cytoplasmic membrane was used as marker for dead cells, while NucBlue (Hoechst 33342) signal was used to determine total cell number. The results show that the hydrogels present a biocompatibility almost identical to that of pure alginate/$Ca^{2+}$ hydrogel, independently of the filler content, thus confirming the biocompatibility of the developed bi-functional electrical and magnetic actuators (Fig. 9).

## 4. Conclusions

Alginate-based hydrogels with encapsulated iron zerovalent nanoparticles that exhibit bi-functional magneto- and electroactive actuator properties are presented as promising actuators materials. The hybrid hydrogels deflect towards the cathode when exposed to an electric field (15 V) or in the direction of the magnetic field when they are in the proximity of a magnet. It has been confirmed that an increase in nanoparticles content (from 0 % to 10 %) positively favours the electromechanical and magnetic response of the material. Unlike other similar systems, these alginate hybrids exhibit excellent mechanical stability and can be printed into three-dimensional actuators that can be operated remotely. Moreover, cytotoxicity tests show high biocompatibility of the gels, revealing their suitability for the development of printable three-dimensional biomimetic dynamic scaffolds and actuators for soft robotics and biomedical applications.

Supplementary data to this article can be found online at https://doi.org/10.1016/j.ijbiomac.2022.07.189.

## Declaration of competing interest

None.

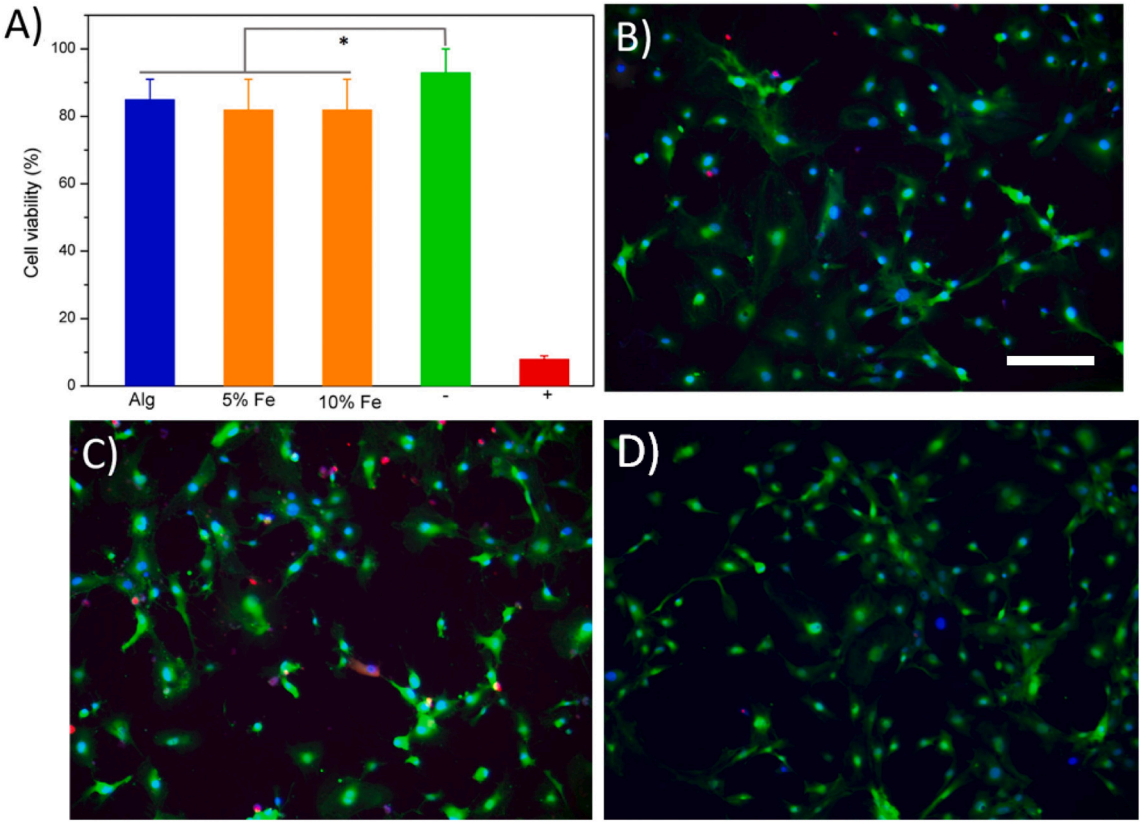


**Fig. 9.** A) Normalized cell viability results. In the positive control conditions, cell membranes were permeabilized by incubation in ice-cold ethanol to allow access to ethidium homodimer. Cells in the negative control were cultured without hydrogel, resulting in high cell viability and increased conversion of calcein-AM to fluorescent calcein. B–D) Fluorescent images corresponding to B) Alginate + 0 % NPs, C) Alginate + 5 % NPs and D) Alginate + 10 % NPs. Blue channel: NucBlue, nuclei; Green channel: calcein, live cells; red channel: ethidium homodimer, dead cells. Scale bar represents 200 μm.

## Data availability

The raw/processed data required to reproduce these findings cannot be shared at this time due to technical or time limitations.

## Acknowledgements

The authors acknowledge funding by Spanish State Research Agency (AEI) and the European Regional Development Fund (ERFD) through the project PID2019-106099RB-C43/AEI/10.13039/501100011033, as well as, from University of the Basque Country UPV/EHU (GIU 207075), and from the Basque Government Industry Department under the ELKARTEK (KK-2021/00040) program. The authors thank Dra. Cristina Eguizabal for giving them access to the Basque Center for Transfusion and Human Tissues at the Galdakao hospital, to perform the biological assays. Technical and human support provided by SGIker (UPV/EHU, MICINN, GV/EJ, EGEF and ESF) is gratefully acknowledged.

## References

[1] J.C. Breger, C. Yoon, R. Xiao, H.R. Kwag, M.O. Wang, J.P. Fisher, T.D. Nguyen, D. H. Gracias, Self- folding thermo-magnetically responsive soft microgrippers, Appl. Mater. Interfaces 7 (2015) 3398–3405, https://doi.org/10.1021/am508621s.
[2] K.T. Nguyen, J.L. West, Photopolymerizable hydrogels for tissue engineering applications, Biomaterials 23 (2002) 4307–4314, https://doi.org/10.1016/S0142-9612(02)00175-8.
[3] L. Klouda, A.G. Mikos, Thermoresponsive hydrogels in biomedical applications -a review, Eur. J. Pharm. Biopharm. 68 (2008) 34–45, https://doi.org/10.1016/j.ejpb.2007.02.025.
[4] J.O. You, D.T. Auguste, Conductive, physiologically responsive hydrogels, Langmuir 26 (2010) 4607–4612, https://doi.org/10.1021/la100294p.
[5] J.Z, Y.M.C.Hussain Haider, Can Hui Yang, Wen Jiang Zheng, Jian Hai Yang, Mei Xiang Wang, Sen Yang, Miklós Zrínyi, Yoshihito Osada, Zhigang Suo, Qiqing Zhang, Exceptionally tough and notch-insensitive magnetic hydrogels, Soft Matter 11 (2015) 8253–8261, https://doi.org/10.1039/C5SM01487E.
[6] G. Kaklamani, D. Kazaryan, J. Bowen, F. Iacovella, S.H. Anastasiadis, G. Deligeorgis, On the electrical conductivity of alginate hydrogels, Regen. Biomater. 5 (2018) 293–301, https://doi.org/10.1093/rb/rby019.
[7] H. Cui, Q. Zhao, L. Zhang, X. Du, Intelligent polymer-based bioinspired actuators: from monofunction to multifunction, Adv. Intell. Syst. 2 (2020), 2000138, https://doi.org/10.1002/aisy.202000138.
[8] A. Pardo, M. Gómez-Florit, S. Barbosa, P. Taboada, R.M.A. Domingues, M. E. Gomes, Magnetic nanocomposite hydrogels for tissue engineering: design concepts and remote actuation strategies to control cell fate, ACS Nano 15 (2021) 175–209, https://doi.org/10.1021/acsnano.0c08253.
[9] Q.Y. Guo, S.Y. Ren, J.Y. Wang, Y. Li, Z.Y. Yao, H. Huang, Z.X. Gao, S.P. Yang, Low field nuclear magnetic sensing technology based on hydrogel-coated superparamagnetic particles, Anal. Chim. Acta 1094 (2020) 151–159, https://doi.org/10.1016/j.aca.2019.10.013.
[10] Z. Li, Y. Li, C. Chen, Y. Cheng, Magnetic-responsive hydrogels: from strategic design to biomedical applications, J. Control. Release 335 (2021) 541–556, https://doi.org/10.1016/j.jconrel.2021.06.003.
[11] S. Maiz-Fernández, L. Pérez-Álvarez, L. Ruiz-Rubio, J.L. Vilas-Vilela, S. Lanceros-Méndez, Multifunctional materials based on smart hydrogels for biomedical and 4D applications, Adv. Light. Multifunct. Mater. (2021) 407–467, https://doi.org/10.1016/b978-0-12-818501-8.00010-x.
[12] K. Cai, J. Zhang, L.H. Deng, L. Yang, Y. Hu, C. Chen, L. Xue, L. Wang, Physical and biological properties of a novel hydrogel composite based on oxidized alginate, gelatin and tricalcium phosphate for bone tissue engineering, Adv. Eng. Mater. 9 (2007) 1082–1088, https://doi.org/10.1002/adem.200700222.
[13] W.S. Kim, D.J. Mooney, P.R. Arany, K. Lee, N. Huebsch, J. Kim, Adipose tissue engineering using injectable, oxidized alginate hydrogels, Tissue Eng. - Part A. 18 (2012) 737–743, https://doi.org/10.1089/ten.tea.2011.0250.
[14] N. Salamatipour, N. Hemmatinejad, A. Bashari, Synthesis of redox-light responsive alginate Nano hydrogel to produce smart textile, Fibers Polym. 20 (2019) 690–697, https://doi.org/10.1007/s12221-019-8905-0.
[15] S. Mallakpour, E. Azadi, C.M. Hussain, State-of-the-art of 3D printing technology of alginate-based hydrogels—an emerging technique for industrial applications, Adv. Colloid Interf. Sci. 293 (2021), 102436, https://doi.org/10.1016/j.cis.2021.102436.
[16] N. Taira, K. Ino, J. Robert, H. Shiku, Electrochemical printing of calcium alginate/gelatin hydrogel, Electrochim. Acta 281 (2018) 429–436, https://doi.org/10.1016/j.electacta.2018.05.124.
[17] M.N.I. Shiblee, K. Ahmed, M. Kawakami, H. Furukawa, 4D printing of shape-memory hydrogels for soft-robotic functions, Adv. Mater. Technol. 4 (2019) 1–10, https://doi.org/10.1002/admt.201900071.
[18] J. Schindelin, I. Arganda-Carreras, E.F. Verena Kaynig, M. Longair, T. Pietzsch, S. Preibisch, C. Rueden, S. Saalfeld, B. Schmid, A. Cardona, Fiji: an open-source platform for biological-image analysis, Nat. Methods 9 (2012) 676–682, https://doi.org/10.1038/nmeth.2019.
[19] S.D. Dutta, J. Hexiu, D.K. Patel, K. Ganguly, K.T. Lim, 3D-printed bioactive and biodegradable hydrogel scaffolds of alginate/gelatin/cellulose nanocrystals for tissue engineering, Int. J. Biol. Macromol. 167 (2021) 644–658, https://doi.org/10.1016/j.ijbiomac.2020.12.011.
[20] N. Bao, X. Miao, X. Hu, Q. Zhang, X. Jie, X. Zheng, Novel synthesis of plasmonic Ag/AgCl@TiO2 continues fibers with enhanced broadband photocatalytic performance, Catalysts. 7 (2017), https://doi.org/10.3390/catal7040117.
[21] G. Lawrie, I. Keen, B. Drew, A. Chandler-temple, L. Rintoul, P. Fredericks, L. Grøndahl, in: Interactions Between Alginate and Chitosan Biopolymers Characterized Using FTIR and XPS, 2007, pp. 2533–2541, https://doi.org/10.1021/bm070014y.
[22] A. Razmjou, M.R. Barati, G.P. Simon, K. Suzuki, H. Wang, Fast deswelling of nanocomposite polymer hydrogels via magnetic field-induced heating for emerging FO, Desalination (2013), https://doi.org/10.1021/es4005152.
[23] J.A. Galicia, F. Cousin, E. Dubois, O. Sandre, V. Cabuil, R. Perzynski, Static and dynamic structural probing of swollen polyacrylamide ferrogels, Soft Matter 5 (2009) 2614–2624, https://doi.org/10.1039/b819189a.
[24] W.P. Voo, C.W. Ooi, A. Islam, B.T. Tey, E.S. Chan, Calcium alginate hydrogel beads with high stiffness and extended dissolution behaviour, Eur. Polym. J. 75 (2016) 343–353, https://doi.org/10.1016/j.eurpolymj.2015.12.029.
[25] W. Chen, P.H.J. Kouwer, Combining mechanical tuneability with function: biomimetic fibrous hydrogels with nanoparticle crosslinkers, Adv. Funct. Mater. 2105713 (2021), 2105713, https://doi.org/10.1002/adfm.202105713.
[26] J. Crangle, G.M. Goodman, The magnetization of pure iron and nickel, Proc. R. Soc. London. A. Math. Phys. Sci. 321 (1971) 477–491, https://doi.org/10.1098/rspa.1971.0044.
[27] I. San Román, A. Galdames, M.L. Alonso, L. Bartolomé, J.L. Vilas, R.M. Alonso, Effect of coating on the environmental applications of zero valent iron nanoparticles: the lindane case, Sci. Total Environ. 565 (2016) 795–803, https://doi.org/10.1016/j.scitotenv.2016.04.034.
[28] Y. Yang, M.W. Urban, Self-healing polymeric materials, Chem. Soc. Rev. 42 (2013) 7446–7467, https://doi.org/10.1039/c3cs60109a.
[29] P.J. Glazer, M. van Erp, A. Embrechts, S.G. Lemay, E. Mendes, Role of pH gradients in the actuation of electro-responsive polyelectrolyte, Soft Matter 8 (2012) 4421–4426, https://doi.org/10.1039/c2sm07435d.